Analytical model of magnetic nanoparticle transport and capture in the microvasculature

E. P. Furlani* and K. C. Ng
Institute for Lasers, Photonics and Biophotonics, University at Buffalo (SUNY), Buffalo, New York, 14260, USA
(Received 21 December 2005; revised manuscript received 24 March 2006; published 27 June 2006)

An analytical model is presented for predicting the transport and capture of therapeutic magnetic nanoparticles in the human microvasculature. The nanoparticles, with surface bound drug molecules, are injected into the vascular system upstream from malignant tissue, and are captured at the tumor site using a local applied magnetic field. The applied field is produced by a rare-earth cylindrical magnet positioned outside the body. An analytical expression is derived for predicting the trajectory of a particle as it flows through the microvasculature in proximity to the magnet. In addition, a scaling relation is developed that enables the prediction of the minimum particle radius required for particle capture. The theory takes into account the dominant magnetic and fluidic forces, which depend on the position and properties of the magnet, the size and magnetic properties of the nanoparticles, the dimensions of the microvessel, the hematocrit level of the blood, and the flow velocity. The model is used to study noninvasive drug targeting, and the analysis indicates that submicron particles can be directed to tumors that are several centimeters from the field source.

DOI: 10.1103/PhysRevE.73.061919 PACS number(s): 87.83.+a, 87.80.Fe, 87.10.+e

I. INTRODUCTION

Magnetic targeting of anticancer agents to malignant tissue using magnetic carrier particles can improve the effectiveness of the treatment while reducing its side effects. The growing interest in this therapy is due to rapid progress in the development of functionalized magnetic nanoparticles that are designed to target a specific tissue, and effect local chemo-, radio-, and genetherapy at a tumor site [1–4]. In magnetic drug targeting, magnetic carrier particles with surface-bound drug molecules are injected into the vascular system upstream from the malignant tissue, and are captured at the tumor via a local applied magnetic field. Upon achieving a sufficient concentration, the drug molecules are released from the carriers by changing physiological conditions such as *p*H, osmolality, or temperature, or by enzymatic activity [5]. The released drug is taken up by the malignant cells, and the magnetic carriers are ultimately processed by the body. Since the therapeutic agents are localized to regions of diseased tissue, higher dosages can be applied which enables more effective treatment. This is in contrast to conventional therapy in which a drug is distributed in a systemic fashion throughout the body, which can have a deleterious affect on healthy tissue

Magnetic drug targeting has been studied primarily using surface tumors [4,5] and small animal models: rabbits [5], swine [6,7], and rats [8,9]. Clinical trials have produced encouraging results that range from the permanent remission of squamous cell carcinoma in New Zealand White Rabbits [5], to the effective treatment of breast cancer in humans [10–12].

In addition to the clinical trials, theoretical research has been conducted to predict magnetic drug targeting for various applications. In most of this work numerical methods such as finite element analysis (FEA) are used to calculate the magnetic field distribution. The numerical field solution is used in the equations of motion to predict the particle trajectory, which is based on Newtonian dynamics [13–16]. The fluidic force on the particle is usually obtained using Stokes' law for the drag on a sphere in a laminar flow field. As a further simplification, the blood flow is often modeled as two-dimensional laminar flow of Newtonian fluid between stationary parallel plates. While these studies are useful for predicting viable operating parameters for magnetic targeting systems, there is a need for a more rigorous theory, preferably one that does not rely on either a numerical field solution, which is awkward for parametric analysis, or a two dimensional flow approximation, which is a poor approximation for flow through a cylindrical vessel.

In this paper we present an analytical model for predicting the transport and capture of magnetic nanoparticles in the microvasculature. Magnetophoretic control of the particles is provided by a rare-earth cylindrical magnet positioned outside the body as shown in Fig. 1. The magnet is assumed to be of infinite extent, with its axis orthogonal to the blood flow. It is magnetized perpendicular to its axis, and produces a nonuniform field distribution in nearby tissue. The magnetic force that it produces is based on an analytical expression for the field distribution in the microvessel, combined

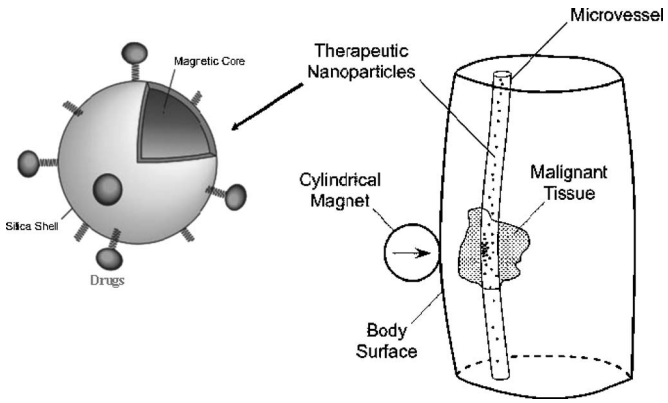

FIG. 1. Noninvasive magnetophoretic drug targeting in a microvessel.

*Corresponding author. Email address: efurlani@buffalo.edu

with a linear magnetization model for the magnetic response of particles. The model takes into account the dimensions and polarization of the magnet, the magnetization and size of the particles, the dimensions of the microvessel, the hematocrit level of the blood, and the flow velocity. The fluidic analysis is based on the assumption of laminar blood flow through a cylindrical microvessel, and the effect of the blood cells is taken into account via use of an effective bulk viscosity. The analytical force expressions are used in the equations of motion, which are solved analytically to predict particle trajectories within a microvessel, parametrically as a function of the variables described above. In addition, a scaling relation is developed that enables the prediction of the minimum particle radius required for particle capture. The model is used to study particle capture, and the analysis demonstrates the viability of using noninvasive magnetophoretic control of magnetic nanoparticles to effect drug delivery to tumors that are a few centimeters from the field source. The model is ideal for parametric optimization of novel magnetophoretic systems for drug delivery, and can be of substantial benefit in improving the effectiveness of magnetic targeting apparatus for clinical research.

II. THEORY

A. Equations of motion

Magnet particle transport in the microvasculature is governed by several factors including (a) the magnetic force due to all field sources, (b) viscous drag, (c) particle–blood-cell interactions, (d) inertia, (e) buoyancy, (f) gravity, (g) thermal kinetics (Brownian motion), (h) particle-fluid interactions (perturbations to the flow field), and (i) interparticle effects that include magnetic dipole interactions, electric double-layer interactions, and van der Walls force. In this paper, we take into account the dominant magnetic and viscous forces, and the particle–blood-cell interactions via use of an effective viscosity. We ignore all other forces, which are second order. For example, the gravitational and buoyant forces F_g and F_b on a 0.5 μm (R_p=250 nm) iron-oxide (Fe_3O_4, ρ =5000 Kg/m^3) particle in water are $F_g=3.2\times10^{-3}$ pN and $F_b=0.641\times10^{-3}$ pN. These are an order of magnitude smaller than the magnetic force. A similar analysis applies to the inertial force $m_p a_p$, which we discuss in more detail below. We assume that we are dealing with dilute particle suspensions in which the particle volume concentration is small, i.e., $c \ll 1$ (c is the total volume occupied by the particles per unit volume of fluid). In this case, interparticle effects and particle-fluid interactions can also be neglected.

We predict particle motion using Newton's law:

$$m_p \frac{d\mathbf{v}_p}{dt} = \mathbf{F}_m + \mathbf{F}_f, \tag{1}$$

where m_p and $\mathbf{v}_p$ are the mass and velocity of the particle, and $\mathbf{F}_m$ and $\mathbf{F}_f$ are the magnetic and fluidic forces, respectively. As noted above, and discussed in more detail later, the inertial term $m_p \frac{d\mathbf{v}_p}{dt}$ is small and could be neglected. The magnetic force is obtained using the "effective" dipole moment method in which the magnetized particle is replaced by an "equivalent" point dipole with a moment $\mathbf{m}_{p,\text{eff}}$ [17]. The force on the dipole (and hence on the particle) is given by

$$\mathbf{F}_m = \mu_f (m_{p,\text{eff}} \cdot \nabla)\mathbf{H}_a, \tag{2}$$

where μ_f is the permeability of the transport fluid, $\mathbf{m}_{p,\text{eff}}$ is the effective dipole moment of the particle, and $\mathbf{H}_a$ is the (externally) applied magnetic field intensity at the center of the particle, were the equivalent point dipole is located. If the particle is in free space, $\mathbf{m}_{p,\text{eff}}=V_p\mathbf{M}_p$ and Eq. (2) reduces to the usual form $\mathbf{F}_m=\mu_0 V_p(\mathbf{M}_p\cdot\nabla)\mathbf{H}_a$, where V_p and M_p are the volume and magnetization of the particle, respectively. The fluidic force is obtained using the Stokes' approximation for the drag on a sphere [18],

$$\mathbf{F}_f = -6\pi\eta R_p(\mathbf{v}_p - \mathbf{v}_f), \tag{3}$$

where η and $\mathbf{v}_f$ are the viscosity and the velocity of the fluid, respectively.

At this point, we digress briefly to discuss the limitations of the Newtonian approach. Equation (1) does not take into account Brownian motion, which can influence particle capture when the particle diameter D_p is sufficiently small. Gerber *et al.* [19] have developed the following criterion to estimate this diameter:

$$|F| D_p \leqslant kT, \tag{4}$$

where $|F|$ is the magnitude of the total force acting on the particle, k is the Boltzmann constant, and T is the absolute temperature. In order to apply Eq. (4), one needs to estimate $|F|$. If the magnetic field source is specified, one can estimate $|F|$ for a given particle by taking a spatial average of the force on the particle over the region of interest. Gerber *et al.* have studied the capture of Fe_3O_4 particles in water using a single magnetic wire, and have estimated the critical particle diameter for this application to be $D_{c,p}\equiv kT/|F|=40$ nm (i.e., $|F|=0.1$ pN) [19]. For particles with a diameter below $D_{c,p}$ (which is application dependent) one solves an advection-diffusion equation for the particle number density $n(\mathbf{r},t)$, rather than the Newtonian equation for the trajectory of a single particle. The behavior of $n(\mathbf{r},t)$ is governed by the following equation [19–21]:

$$\frac{\partial n(\mathbf{r},t)}{\partial t} + \nabla\cdot\mathbf{J} = 0, \tag{5}$$

where $\mathbf{J}=\mathbf{J}_D+\mathbf{J}_F$ is the total flux of particles, which includes a contribution $\mathbf{J}_D=-D\nabla n(\mathbf{r},t)$ due to diffusion, and a contribution $\mathbf{J}_F=\mathbf{v}n(\mathbf{r},t)$ due to the action of all external forces. Equation (5) is often written in terms of the particle volume concentration $c(\mathbf{r},t)$, which is related to the number density, $c(\mathbf{r},t)=4\pi R_p^3 n(\mathbf{r},t)/3$. The diffusion coefficient D is given by the Nernst-Einstein relation $D=\mu kT$, where $\mu=1/(6\pi\eta R_p)$ is the mobility of a particle of radius R_p in a fluid with viscosity η (Stokes' approximation). The drift velocity also depends of the mobility $\mathbf{v}(\mathbf{r})=\mu\mathbf{F}(\mathbf{r})$, where $\mathbf{F}(r)=\mathbf{F}_m(r)+\mathbf{F}_f(r)+\cdots$ is the total force on the particle. Thus Eq. (5) can be rewritten as

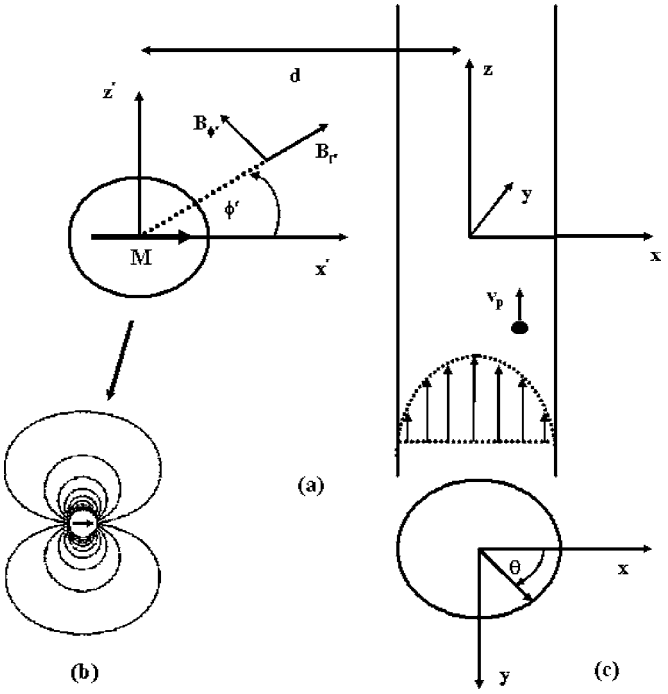

FIG. 2. Geometry and reference frame for analysis: (a) coordinate systems and reference frames, (b) magnetic flux lines for a cylindrical magnet, cross section of microvessel with reference frame.

$$\frac{\partial n(\mathbf{r},t)}{\partial t} = \frac{kT}{(6\pi\eta R_p)}\nabla^2 n(\mathbf{r},t) - \frac{1}{(6\pi\eta R_p)}\nabla \cdot (\mathbf{F}(\mathbf{r})n(\mathbf{r},t)). \tag{6}$$

B. Magnetic force

To determine the magnetic force, we need a model for the magnetic response of the particle. We use a linear magnetization model with saturation. Specifically, below saturation,

$$\mathbf{M}_p = \chi_p \mathbf{H}_{\text{in}}, \tag{7}$$

where μ_p and $\chi_p = \mu_p/\mu_0 - 1$ are permeability and susceptibility of the particle. Above saturation $\mathbf{M}_p = \mathbf{M}_{\text{sp}}$, where $\mathbf{M}_{\text{sp}}$ is the saturation magnetization of the particle. In Eq. (7), $\mathbf{H}_{\text{in}} = \mathbf{H}_a - \mathbf{H}_{\text{demag}}$ is the field inside the particle, which is different than the (externally) applied field, because the magnetization of the particle itself gives rise to a self-demagnetization field $\mathbf{H}_{\text{demag}}$ that opposes $\mathbf{H}_a$ (see pp. 23–27 in Ref. [22]). For example, for a uniformly magnetized sphere with magnetization $\mathbf{M}_p$ in free space, $\mathbf{H}_{\text{damag}} = \frac{\mathbf{M}_p}{3}$ is the field inside the sphere due to the "magnet change" $\sigma_m = \mathbf{M}_p \cdot \hat{n}$ at its surface ($\hat{n}$ is the unit vector normal to the surface). According to the linear model, the magnetic field intensity required to saturate the particle is $\mathbf{H}_{\text{in,sat}} = \mathbf{M}_{\text{sp}}/\chi_p$.

We now determine the magnetic force using the "effective" dipole moment method as described by Jones [17]. The effective moment of the particle (the equivalent point dipole moment) is obtained as follows: (i) first solve the magnetostatic boundary value problem for the particle (sphere) immersed in a fluid, with its magnetization $\mathbf{M}_p$ parallel to the applied field; and then (ii) determine the equivalent point dipole moment $\mathbf{m}_{p,\text{eff}}$ that, when positioned at the center of the particle, produces the same field distribution outside the particle as that produced by the particle itself.

The fields inside and outside the particle can be represented in terms of scalar potentials, $\Phi_{in} = -\nabla H_{in}$ and $\Phi_{out} = -\nabla H_{out}$ where

$$\Phi_{in}(r,\theta) = -C_{in} r\cos(\theta) \quad (r < R_p), \tag{8}$$

$$\Phi_{out}(r,\theta) = -H_a r\cos(\theta) + C_{out}\frac{\cos(\theta)}{r^2} \quad (r \geq R_p). \tag{9}$$

In Eqs. (8) and (9), (r,θ) are spherical polar coordinates taken with respect to the center of the particle, with the z axis in the direction of the applied field. It is instructive to note that the magnitude of the field intensity inside the particle is $H_{in,z} = -[\partial_r \Phi_{in}(r,\theta)]\cos(\theta) + \frac{1}{r}[\partial_r \Phi_{in}(r,\theta)]\sin(\theta) = C_{in}$. The unknown coefficients C_{in} and C_{out} are obtained from the boundary conditions for the potential $\Phi_{in}(r,\theta) = \Phi_{out}(r,\theta)$, and for the normal component of $\mathbf{B} = \mu_0(\mathbf{H}+\mathbf{M})$, $\mu_0(-\partial_r \Phi_{in} + M_p) = -\mu_f \partial_r \Phi_{out}$, which are evaluated at $r = R_p$. These give

$$C_{in} = \frac{3\mu_f}{\mu_0 + 2\mu_f} H_a - \frac{\mu_0}{\mu_0 + 2\mu_f} M_p, \tag{10}$$

and

$$C_{out} = \frac{\mu_0 - \mu_f}{\mu_0 + 2\mu_f} R_p^3 H_a + \frac{\mu_0}{\mu_0 + 2\mu_f} R_p^3 M_p. \tag{11}$$

Now, the potential due to a point dipole of magnitude $m_{p,\text{eff}}$ is of the form

$$\Phi_{eff} = m_{p,\text{eff}} \frac{\cos(\theta)}{4\pi r^2}. \tag{12}$$

Thus by comparing Eqs. (9) and (12) we find that the magnitude of the "equivalent" dipole for the particle is $m_{p,\text{eff}} = 4\pi C_{out}$, and from Eq. (11) we have

$$m_{p,\text{eff}} = 4\pi R_p^3 \left[\frac{\mu_0 - \mu_f}{\mu_0 + 2\mu_f} H_a + \frac{\mu_0}{\mu_0 + 2\mu_f} M_p \right]. \tag{13}$$

Since $H_{in} = C_{in}$, we also find that

$$H_{in} = \frac{3\mu_f}{\mu_0 + 2\mu_f} H_a - \frac{\mu_0}{\mu_0 + 2\mu_f} M_p. \tag{14}$$

Now, if the particle is below saturation, $M_p = \chi_p H_{in}$. We substitute this into Eqs. (13) and (14) and obtain

$$H_{in} = \frac{3(\chi_f + 1)}{[(\chi_p - \chi_f) + 3(\chi_f + 1)]} H_a, \tag{15}$$

and

$$M_p = \frac{3\chi_p(\chi_f + 1)}{[(\chi_p - \chi_f) + 3(\chi_f + 1)]} H_a, \tag{16}$$

and

$$m_{p,\mathrm{eff}} = V_p \frac{3(\chi_p - \chi_f)}{[(\chi_p - \chi_f) + 3(\chi_f + 1)]} H_a, \tag{17}$$

where V_p is the volume of the particle. Finally, we substitute Eq. (17) into Eq. (2) and obtain the force on the magnetized particle in a fluid of permeability μ_f,

$$\mathbf{F}_m = \mu_f V_p \frac{3(\chi_p - \chi_f)}{[(\chi_p - \chi_f) + 3(\chi_f + 1)]} (\mathbf{H}_a \cdot \nabla)\mathbf{H}_a. \tag{18}$$

Now, when $|\chi_f| \ll 1$ (i.e., $\mu_f \approx \mu_0$), Eq. (18) reduces to

$$\mathbf{F}_m = \mu_0 V_p \frac{3(\chi_p - \chi_f)}{(\chi_p - \chi_f) + 3} (\mathbf{H}_a \cdot \nabla)\mathbf{H}_a. \tag{19}$$

It also follows that

$$\mathbf{H}_{\mathrm{in}} = \frac{3}{(\chi_p - \chi_f) + 3} \mathbf{H}_a, \tag{20}$$

and that

$$\mathbf{m}_{p,\mathrm{eff}} = V_p \frac{3(\chi_p - \chi_f)}{(\chi_p - \chi_f) + 3} \mathbf{H}_a. \tag{21}$$

If we take saturation into account, the effective dipole moment can be written as

$$\mathbf{m}_{p,\mathrm{eff}} = V_p f(H_a) \mathbf{H}_a, \tag{22}$$

where

$$f(H_a) = \begin{cases} \dfrac{3(\chi_p - \chi_f)}{(\chi_p - \chi_f) + 3} & H_a < \left(\dfrac{(\chi_p - \chi_f) + 3}{3\chi_p} \right) M_{\mathrm{sp}} \\ M_{\mathrm{sp}}/H_a & H_a \geqslant \left(\dfrac{(\chi_p - \chi_f) + 3}{3\chi_p} \right) M_{\mathrm{sp}} \end{cases} \quad (|\chi_f| \ll 1), \tag{23}$$

and $H_a = |\mathbf{H}_a|$.

In this analysis, the magnet is assumed to be of infinite extent in the y direction, and therefore the y components of the magnetic field and force are zero, i.e.,

$$\mathbf{H}_a = H_{ax}(x,z)\hat{\mathbf{x}} + H_{az}(x,z)\hat{\mathbf{z}}, \tag{24}$$

and

$$\mathbf{F}_m(x,z) = F_{mx}(x,z)\hat{\mathbf{x}} + F_{mz}(x,z)\hat{\mathbf{z}}, \tag{25}$$

where

$$F_{mx}(x,z) = \mu_0 V_p f(H_a) \left[H_{ax}(x,z) \frac{\partial H_{ax}(x,z)}{\partial x} + H_{az}(x,z) \frac{\partial H_{ax}(x,z)}{\partial z} \right], \tag{26}$$

and

$$F_{mz}(x,z) = \mu_0 V_p f(H_a) \left[H_{ax}(x,z) \frac{\partial H_{az}(x,z)}{\partial x} + H_{az}(x,z) \frac{\partial H_{az}(x,z)}{\partial z} \right]. \tag{27}$$

To evaluate $\mathbf{F}_m(x,y)$ we need an expression for the field distribution $\mathbf{H}_a(x,y)$.

C. Magnetic field and force of a cylindrical magnet

The source magnet has a radius R_{mag} and is centered with respect to the origin in the x'-z' plane as shown in Fig. 2. The magnet is magnetized to a level M_s through its cross-section, and its field components in cylindrical coordinates are (p. 179 of Ref. [17])

$$H_{r'}(r',\phi') = \frac{M_s}{2} \frac{R_{mag}^2}{r'^2} \cos(\phi'), \tag{28}$$

and

$$H_{\phi'}(r',\phi') = \frac{M_s}{2} \frac{R_{mag}^2}{r'^2} \sin(\phi'). \tag{29}$$

We convert these to Cartesian coordinates,

$$H_{x'}(x',z') = \frac{M_s R_{mag}^2}{2} \frac{(x'^2 - z'^2)}{(x'^2 + z'^2)^2}, \tag{30}$$

$$H_{z'}(x',z') = \frac{M_s R_{mag}^2}{2} \frac{2x'z'}{(x'^2 + z'^2)^2}, \tag{31}$$

and obtain the field gradients,

$$\frac{\partial H_{x'}(x',z')}{\partial x'} = \frac{M_s R_{mag}^2 x'(3z'^2 - x'^2)}{(x'^2 + z'^2)^3}, \tag{32}$$

$$\frac{\partial H_{x'}(x',z')}{\partial z'} = \frac{M_s R_{mag}^2 z'(z'^2 - 3x'^2)}{(x'^2 + z'^2)^3}, \tag{33}$$

$$\frac{\partial H_{z'}(x',z')}{\partial x'} = \frac{M_s R_{mag}^2 z'(z'^2 - 3x'^2)}{(x'^2 + z'^2)^3}, \tag{34}$$

$$\frac{\partial H_{z'}(x',z')}{\partial z'} = \frac{M_s R_{mag}^2 x'(x'^2 - 3z'^2)}{(x'^2 + z'^2)^3}. \quad (35)$$

For the force analysis, we rewrite Eqs. (32)–(35) in terms of the (x,z) coordinates that are fixed with respect to the microvessel [Fig. 2(a)]. Specifically, we transform Eqs. (30)–(35), substitute into Eqs. (26) and (27), and obtain

$$F_{mx} = -\mu_0 V_p f(H_a) M_s^2 R_{mag}^4 \frac{(x+d)}{2[(x+d)^2 + z^2]^3}, \quad (36)$$

and

$$F_{mz} = -\mu_0 V_p f(H_a) M_s^2 R_{mag}^4 \frac{z}{2[(x+d)^2 + z^2]^3}. \quad (37)$$

The force component that governs particle capture is F_{mx}, and from Eq. (36) we find that it is always attractive (towards the magnet) as $d \gg x$.

D. Fluidic force

To evaluate the fluidic force in Eq. (3) we need an expression for the fluid velocity $\mathbf{v}_f$ in a microvessel. We choose a coordinate system with the z axis along the axis of the vessel, and with the x-y plane centered with respect to its cross section. We assume fully developed laminar flow parallel to the z axis,

$$v_f(x,y) = 2\bar{v}_f \left[1 - \left(\frac{(x^2+y^2)^{1/2}}{R_v} \right)^2 \right], \quad (38)$$

where $\bar{v}_f$ is the average axial fluid velocity in a microvessel of radius R_v. We substitute Eq. (38) into Eq. (3) and obtain the fluidic force components

$$\mathbf{F}_{\mathrm{fx}} = -6\pi\eta R_p v_x, \quad (39)$$

$$\mathbf{F}_{\mathrm{fy}} = -6\pi\eta R_p v_y, \quad (40)$$

and

$$\mathbf{F}_{\mathrm{fz}} = -6\pi\eta R_p \left\{ v_z - 2\bar{v}_f \left[1 - \left(\frac{(x^2+y^2)^{1/2}}{R_v} \right)^2 \right] \right\}. \quad (41)$$

To evaluate Eqs. (39)–(41) we need an expression for blood viscosity η. Blood is a suspension of red and white blood cells (erythrocytes and leukocytes), and platelets in plasma. Blood plasma (absent the cells and platelets) is an incompressible Newtonian fluid with a viscosity $\eta_{plasma} = 0.0012$ N s/m^2. Red blood cells have a biconcave discoid shape with a diameter of 6–8 μm, and a thickness of 2 μm. These cells account for approximately 99% of the particulate matter in blood. The hematocrit, which is the percentage by volume of packed red blood cells in a given sample of blood, is nominally 40–45 %. The rheological properties of blood in the microvasculature depend on many factors including the diameter of the blood vessel, the flow velocity, the hematocrit, the finite size of the blood cells, their elastic properties, the aggregation and deformation of the blood cells, etc. [23]. A rigorous prediction of these properties is beyond the scope of this work. Here, we use an analytical empirically based expression for the viscosity η *in vivo* that applies for medium to high shear rates,

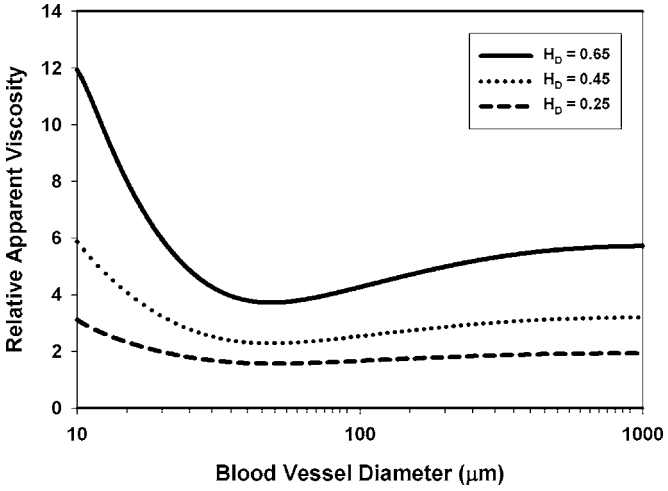

FIG. 3. Relative apparent viscosity vs blood vessel diameter and hematocrit.

$$v_f/D > 50/s. \quad (42)$$

Specifically, the apparent blood viscosity (relative to that of plasma) can be estimated using [24]

$$\eta_{rel} = \left[1 + (\eta_{0.45} - 1) \frac{(1-H_D)^C - 1}{(1-0.45)^C - 1} \left(\frac{D}{D-1.1} \right)^2 \right] \times \left(\frac{D}{D-1.1} \right)^2. \quad (43)$$

In Eq. (43), D is the diameter of the vessel in microns, H_D is the hematocrit (nominally 0.45), and

$$\eta_{0.45} = 6e^{-0.085D} + 3.2 - 2.44e^{-0.06D^{0.645}}, \quad (44)$$

and

$$C = (0.8 + e^{-0.075D}) \left(\frac{1}{1 + 10^{-11} \cdot D^{12}} - 1 \right) + \frac{1}{1 + 10^{-11} \cdot D^{12}}. \quad (45)$$

Parametric plots of η_{rel} are shown in Fig. 3. More extensive plots can be found in Ref. [24]. Notice that η_{rel} decreases with vessel diameter, and obtains a minimum value for diameters between 10 and 100 μm. This is known as the Fahraeus-Lindqvist effect and is due to the fact that blood cells are displaced towards the axis of a narrow vessel as they pass through it thereby creating a cell-depleted region near the wall of the vessel and a relatively fast moving core of cells near the center, which results in a decrease in apparent viscosity. It is important to note that Eq. (43) gives the viscosity relative to that of the plasma. Thus the effective blood viscosity η in Eqs. (39)–(41) is given by

$$\eta = \eta_{rel} \eta_{plasma}. \quad (46)$$

E. Analytical equation for particle motion

The equations of motion can be written in component form by substituting Eqs. (36), (37), and (39)–(41) into Eq. (1),

$$m\frac{dv_x}{dt} = -\mu_0 V_p f(H_a) M_s^2 R_{mag}^4 \frac{(x+d)}{2[(x+d)^2+z^2]^3} - 6\pi\eta R_p v_x, \tag{47}$$

$$m\frac{dv_y}{dt} = -6\pi\eta R_p v_y, \tag{48}$$

and

$$m\frac{dv_z}{dt} = -\mu_0 V_p f(H_a) M_s^2 R_{mag}^4 \frac{z}{2((x+d)^2+z^2)^3} - 6\pi\eta R_p\left[v_z - 2\bar{v}_f\left(1-\frac{x^2+y^2}{R_v^2}\right)\right]. \tag{49}$$

Since the magnetic force has no y-component, we can simplify the analysis by assuming that there is no motion in the y-direction, which means that we ignore Eq. (48), and focus instead on Eqs. (47) and (49) with $y=0$, which govern motion in the x-z plane. These equations can be further simplified. To this end, we scale the distance d (from the magnet to the microvessel) in terms of the magnet radius, $d=(1+\alpha)R_{mag}$, and introduce the dimensionless parameters,

$$\bar{x} = \frac{x}{R_v},$$

$$\bar{z} = \frac{z}{(1+\alpha)R_{mag}},$$

$$\bar{t} = \frac{t2\bar{v}_f}{(1+\alpha)R_{mag}},$$

$$\bar{v}_x = v_x\frac{(1+\alpha)R_{mag}}{2\bar{v}_f R_v},$$

$$\bar{v}_z = \frac{v_z}{2\bar{v}_f}. \tag{50}$$

Using these definitions, Eqs. (47) and (49) can be rewritten in nondimensional form,

$$\bar{m}\frac{d\bar{v}_x}{d\bar{t}} = -C\frac{\beta\bar{x}+1}{[(\beta\bar{x}+1)^2+\bar{z}^2]^3} - \bar{v}_x, \tag{51}$$

$$\bar{m}\frac{d\bar{v}_z}{d\bar{t}} = -C\beta\frac{\bar{z}}{[(\beta\bar{x}+1)^2+\bar{z}^2]^3} - [\bar{v}_z - (1-\bar{x}^2)], \tag{52}$$

where

$$C = \frac{\mu_0 R_p^2 f(H_a) M_s^2}{18\eta R_v \bar{v}_f (1+\alpha)^4}, \tag{53}$$

and

$$\bar{m} = \frac{4\bar{v}_f \rho_p R_p^2}{9\eta(1+\alpha)R_{mag}}, \tag{54}$$

and

$$\beta = \frac{R_v}{(1+\alpha)R_{mag}}. \tag{55}$$

For practical applications, it is easy to verify that $\bar{m} \ll 1$, which implies that inertial effects are negligible. Thus we can neglect the first term in Eq. (51). Similarly, $\beta \ll 1$, which implies that viscous drag dominates motion in the z direction. Thus we also ignore the first term on the right-hand side of Eq. (52), and Eqs. (51) and (52) reduce to

$$\frac{d\bar{x}}{d\bar{t}} = -C\frac{1}{(1+\bar{z}^2)^3}, \tag{56}$$

and

$$\frac{d\bar{z}}{d\bar{t}} = (1-\bar{x}^2). \tag{57}$$

We divide Eq. (56) by Eq. (57),

$$\frac{d\bar{x}}{d\bar{z}} = -\frac{C}{(1+\bar{z}^2)^3(1-\bar{x}^2)}, \tag{58}$$

and integrate Eq. (58) to obtain an analytical equation for the particle trajectory,

$$\left(\bar{x}-\frac{\bar{x}^3}{3}\right) = \left(\bar{x}_0-\frac{\bar{x}_0^3}{3}\right) - C\left[\frac{3}{8}[\tan^{-1}(\bar{z})-\tan^{-1}(\bar{z}_0)] + \frac{1}{8}\left(\frac{\bar{z}(3\bar{z}^2+5)}{(1+\bar{z}^2)^2} - \frac{\bar{z}_0(3\bar{z}_0^2+5)}{(1+\bar{z}_0^2)^2}\right)\right], \tag{59}$$

where $\bar{x}_0$ and $\bar{z}_0$ are the initial normalized coordinates of the particle. Note that we have ignored the spatial dependence of $f(H_a)$ in the parameter C. This amounts to assuming that the particles are either magnetically biased below saturation, or magnetically saturated, throughout their range of motion. These conditions can be tested by evaluating the magnitude of the magnetic field along the axis of the microvessel, and applying Eq. (23). For noninvasive drug targeting the particles are typically biased below saturation.

Equation (59) is an analytical expression for predicting particle motion within a microvessel, and is one of our key results. It is convenient to rewrite it as

$$\bar{x}^3 - 3\bar{x} + 3f(\bar{x}_0,\bar{z}_0,\bar{z}) = 0, \tag{60}$$

where

$$f(\bar{x}_0,\bar{z}_0,\bar{z}) = \left(\bar{x}_0-\frac{\bar{x}_0^3}{3}\right) - C\left[\frac{3}{8}[\tan^{-1}(\bar{z})-\tan^{-1}(\bar{z}_0)] + \frac{1}{8}\left(\frac{\bar{z}(3\bar{z}^2+5)}{(1+\bar{z}^2)^2} - \frac{\bar{z}_0(3\bar{z}_0^2+5)}{(1+\bar{z}_0^2)^2}\right)\right]. \tag{61}$$

Equation (60) can be solved explicitly for $\bar{x}$ in terms of $\bar{z}$. Specifically, for a given value of $\bar{z}$ it has three roots $\bar{x}_1$, $\bar{x}_2$, and $\bar{x}_3$, one of which is physical,

$$\bar{x}_1 = S + T, \tag{62}$$

$$\bar{x}_2 = -\frac{1}{2}[(S+T) - i\sqrt{3}(S-T)], \tag{63}$$

$$\bar{x}_3 = -\frac{1}{2}[(S+T) + i\sqrt{3}(S-T)], \tag{64}$$

where

$$S = \sqrt[3]{\hat{R} + \sqrt{\hat{R}^2 - 1}}, \quad T = \sqrt[3]{\hat{R} - \sqrt{\hat{R}^2 - 1}}, \tag{65}$$

and

$$\hat{R} = -\frac{3}{2} f(\bar{x}_0, \bar{z}_0, \bar{z}). \tag{66}$$

The physical solution of Eq. (60), which we denote as $\bar{x}(\bar{z})$, is real-valued with $|\bar{x}| \leqslant 1$ and satisfies the initial condition $\bar{x}(\bar{z}_0) = \bar{x}_0$. We use Eq. (60) to study particle capture. A particle is captured when its position equals the radius of the blood vessel, i.e., when $\bar{x}^2 = 1$. Let $\bar{z}_c$ denote the normalized point of capture, then $\bar{x}^2(\bar{z}_c) = 1$, or $\bar{x}(\bar{z}_c) = \pm 1$. If a particle is captured, a unique physical solution will exist for $\bar{z}_0 \leqslant \bar{z} \leqslant \bar{z}_c$. If the particle is too small to be captured, a unique physical solution with $|\bar{x}(\bar{z})| < 1$ will exist for $\bar{z}_0 \leqslant \bar{z} < \infty$.

We can estimate the conditions for particle capture as follows. First, we obtain a bound for Eq. (58),

$$\left(\bar{x} - \frac{\bar{x}^3}{3}\right) - \left(\bar{x}_0 - \frac{\bar{x}_0^3}{3}\right) = -C\int_{\bar{z}_0}^{\bar{z}} \frac{d\bar{z}}{(1+\bar{z}^2)^3} > \frac{-C3\pi}{8}. \tag{67}$$

Next, assume that the particle starts at top of the blood vessel (farthest from the magnet) at $\bar{x}_0 = 1$, which gives

$$\left(\bar{x} - \frac{\bar{x}^3}{3}\right) > \frac{2}{3} - \frac{C3\pi}{8}. \tag{68}$$

Now, evaluate Eq. (68) for the condition of particle capture ($\bar{x} = -1$), and obtain

$$C > \frac{32}{9\pi}, \tag{69}$$

or

$$\frac{\mu_0 \pi R_p^2 f(H_a) M_s^2}{64 \eta \bar{v}_f R_v (1+\alpha)^4} > 1. \tag{70}$$

Lastly, we assume that the particle has a susceptibility much greater than that of blood ($\chi_p \gg \chi_f$), and that it is magnetically biased below saturation, which gives

$$\frac{\mu_0 \pi R_p^2 3[\chi_p/(\chi_p+3)] M_s^2}{64 \eta \bar{v}_f R_v (1+\alpha)^4} > 1. \tag{71}$$

It is important to note that the scaling relation (71) is based on the assumption that $\bar{z}_0 = -\infty$. For practical applications this means the particle starts far enough upstream where the magnetic field and force are negligible. Equation (71) can be used determine viable values for the parameters R_p, χ_p, M_s, and α, for achieving efficient particle capture.

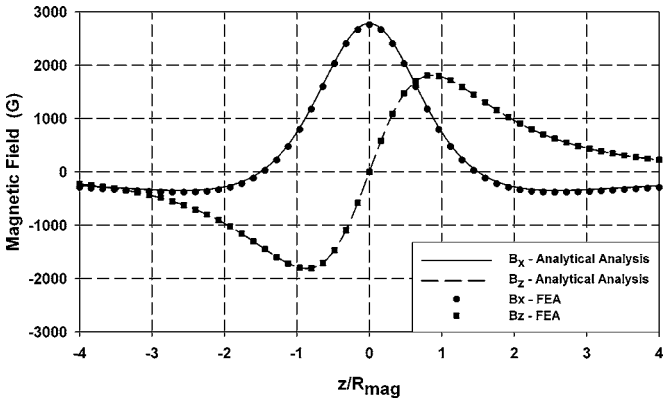

FIG. 4. Magnetic field components along the axis of a microvessel (analytical vs FEA analysis).

III. RESULTS

We use Eq. (60) to study the transport and capture of therapeutic magnetite (Fe_3O_4) nanoparticles in the microvasculature. For this analysis, we assume that the susceptibility of blood is essentially that of free space, but it is important to note that in general, the susceptibility of the suspending medium can have a significant effect on the magnetic force [25–27]. Fe_3O_4 particles are biocompatible, and have a density $\rho_p = 5000\ \mathrm{kg/m^3}$, and a saturation magnetization $M_{sp} = 4.78 \times 10^5\ \mathrm{A/m}$. We adopt a magnetization model for Fe_3O_4 described by Takayasu *et al.* [20], which is consistent with Eq. (23) when $\chi_p \gg 1$,

$$f(H_a) = \begin{cases} 3 & H_a < M_{\mathrm{sp}}/3 \\ M_{\mathrm{sp}}/H_a & H_a \geqslant M_{\mathrm{sp}}/3 \end{cases}. \tag{72}$$

According to this model, if the particle is below saturation then $\mathbf{H}_{\mathrm{demag}} \approx \mathbf{H}_a$ ($\mathbf{H}_{\mathrm{in}} \approx 0$), and $\mathbf{M}_p = 3\mathbf{H}_a$. This model is consistent with a reported volume susceptibility $\chi_{Fe_3O_4}$ for magnetite of between 1 and 6. The reported values for $\chi_{Fe_3O_4}$ are different than the value used here for χ_p because $\chi_{Fe_3O_4}$ is measured with respect to the applied field, rather than the internal field [28]. Throughout this analysis we use the Cartesian coordinate system fixed to the microvessel as shown in Fig. 2 (i.e., the z axis is along the axis of the microvessel).

First, we use Eqs. (30) and (31), and Eqs. (36) and (37) to compute the magnet field and force along the axis of the microvessel ($-4R_{\mathrm{mag}} \leqslant z \leqslant 4R_{mag}$) which is located 1.5 cm from the surface of a rare-earth NdFeB magnet. The magnet is 4 cm in diameter ($R_{mag} = 2.0$ cm, $d = 3.5$ cm) with a magnetization $M_s = 1 \times 10^6$ A/m (remanence $B_r = 1.256$ T). The force is computed on a Fe_3O_4 nanoparticle with a radius $R_p = 100$ nm. Plots of B_x, B_z, F_{mx}, and F_{mz}, along with corresponding data obtained using finite element analysis (FEA), are shown in Figs. 4 and 5. The FEMLAB program from COMSOL was used for the FEA. Notice that B_x obtains its maximum value at the center of the magnet ($z/R_{mag} = 0$), whereas B_z peaks at the edges ($z/R_{mag} = \pm 1$), and alternates

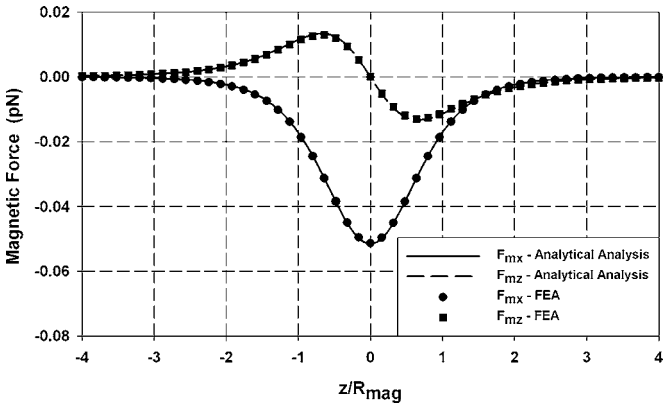

FIG. 5. Magnetic force components on a Fe_3O_4 nanoparticle (analytical vs FEA analysis).

in sign from one edge to the other. The horizontal component of the magnetic force F_{mz} has a profile similar to B_z, but with an opposite polarity of sign (Fig. 5). Thus, as a particle moves horizontally above the magnet (left-to-right) it experiences a horizontal acceleration as it passes the leading edge of the magnet, followed by a deceleration as it passes the trailing edge. The vertical force F_{mx}, which is responsible for particle capture, is always negative (attractive towards the magnet), and is strongest above the center of the magnet ($z/R_{mag}=0$).

Next, we study particle transport through a microvessel. To demonstrate the theory, we choose a microvessel with a radius $R_v=75\ \mu$m, and an average flow velocity $\bar{v}_f=15$mm/s (shear rate $\bar{v}_f/D_v=100/s$). For the calculation of effective viscosity, we assume $\eta_{plasma}=0.0012$ N s/m^2, and a hematocrit of 45%. We use the same magnet parameters above. The initial conditions for the particles are as follows. They start on the axis of the microvessel ($\bar{x}_0=\bar{y}_0=0$), far enough upstream so that the magnetic force is initially negligible, at $z(0)=-4R_{mag}$ [$\bar{z}_0=-4/(1+\alpha)$]. Thus they have an initial velocity equal to the axial flow velocity (i.e., $v_x(0)=0$, $v_y(0)=0$, and $v_z(0)=2\bar{v}_f=30$ mm/s).

We predict the trajectories of five different sized Fe_3O_4 particles: $R_p=150$, 200, 250, 300, 350 nm, for a range of magnet-to-vessel distances $d=(1+\alpha)R_{\mathrm{mag}}$ where $\alpha=0.25$, 0.5, and 0.75. In these plots the radial position $r=|x|$ of the particle is normalized with respect to the microvessel radius R_v, and the axial position z is normalized with respect to the magnet radius R_{mag}. The $\alpha=0.25$ trajectory, along with the magnetic geometry, is shown in Fig. 6. This plot shows that all the particles except the smallest ($R_p=150$ nm) are captured by the magnet when the microvessel is 0.5 cm from the surface of the magnet [$d=(1+\alpha)R_{\mathrm{mag}}=2.5$ cm]. The $\alpha=0.5$ and 0.75 trajectories are shown in Fig. 7. Notice that as the distance from the magnet increases, fewer particles are captured, and at $d=3.5$ cm ($\alpha=0.75$) only the largest particle ($R_p=350$ nm) is captured. This is because the magnetic force is proportional to the volume of the particle ($V_p \propto R_p^3$). Hence larger particles experience a stronger capture force, and can be captured at farther distances. We study the particle size and capture dependency in more detail by analyzing the trajectories of five larger Fe_3O_4 particles: $R_p=400$, 450, 500,

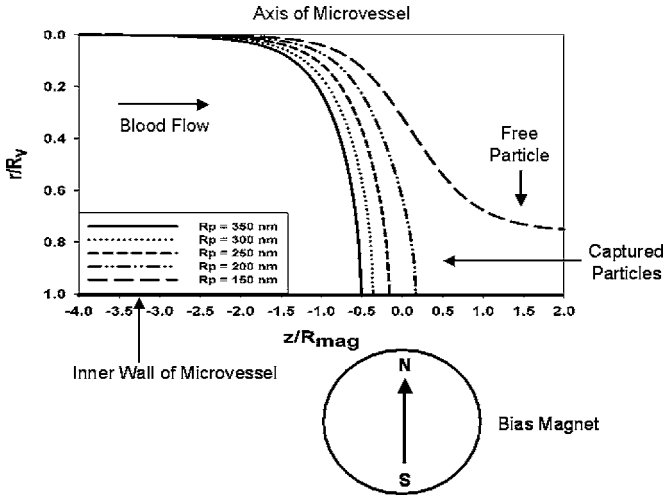

FIG. 6. Trajectories of Fe_3O_4 nanoparticles in a microvessel with $\alpha=0.25$ (cross section of bias magnet shown for reference).

550 and 600 nm, with the microvessel farther from the magnet, i.e., $\alpha=1.0$ and 1.25 (Fig. 8). As before, larger particles are captured at farther distances.

We can estimate the minimum particle radius that will result in capture using Eq. (71) The minimum capture radius depends on the initial position $\bar{x}_0$, $\bar{y}_0$, and $\bar{z}_0$ of the particle. As for the $\bar{z}_0$ dependence, the derivation of the inequality Eq. (71) is based on the assumption that $\bar{z}_0=-\infty$. For practical applications this means the particle starts far enough upstream where the magnetic field and force are negligible. From our analysis above, this occurs when $z_0<-4R_{mag}$, or $\bar{z}_0<-4/(1+\alpha)$. In the following, we assume that this condi-

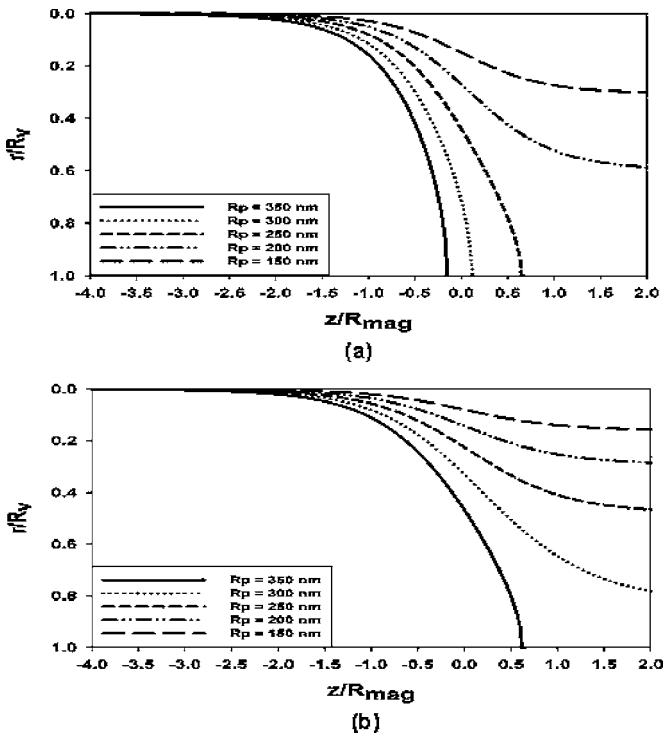

FIG. 7. Trajectories of Fe_3O_4 nanoparticles in a microvessel: (a) $\alpha=0.5$, (b) $\alpha=0.75$.

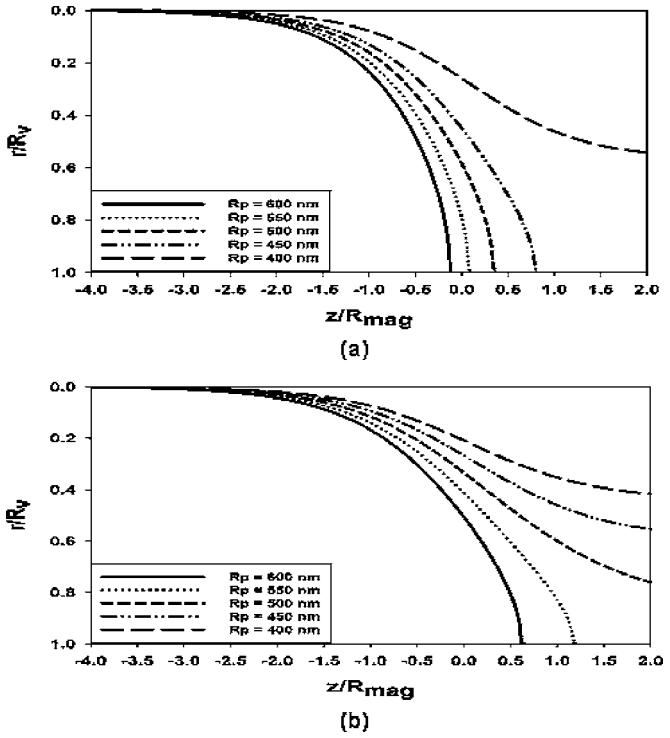

FIG. 8. Trajectories of Fe_3O_4 nanoparticles in a microvessel: (a) $\alpha=1.0$, (b) $\alpha=1.25$.

tion is satisfied. Now, for particles that start at the top of the microvessel ($\bar{x}_0=1$, $\bar{y}_0=0$), farthest from the magnet, we have

$$R_{p,\text{capture}} = \frac{(1+\alpha)^2}{M_s}\sqrt{\frac{64\eta\bar{v}_f R_v}{\mu_0 3\pi}} \quad (\bar{x}_0 = 1). \tag{73}$$

A similar analysis applies to particles that start on the axis of the microvessel ($\bar{x}_0=0$), and yields

$$R_{p,\text{capture}} = \frac{(1+\alpha)^2}{M_s}\sqrt{\frac{32\eta\bar{v}_f R_v}{\mu_0 3\pi}} \quad (\bar{x}_0 = 0). \tag{74}$$

To obtain Eqs. (73) and (74), we have used $\chi_p/(\chi_p+3)\simeq 1$. We evaluate these equations for a range of values $0.25\leqslant\alpha\leqslant 2.5$ (Fig. 9). The values obtained for the $\bar{x}_0=0$ case are consistent with the trajectory analysis above. Specifically, from Eq. (74) we find that the minimum particle radius required to ensure particle capture is $R_{p,\text{capture}}=156$ 225, 305, 400, and 505 nm for $\alpha=0.25$, 0.5, 0.75, 1.0, and 1.25, respectively. From the trajectory analysis, we found that particles with a corresponding radius of $R_p=150$, 200, 300, 400, and 500 nm or below, were not captured, which is consistent.

Lastly, note from Eq. (73) that the minimum particle radius required for capture does not depend on the distance to the capture site *per se*, but rather on the ratio d^2/R_{mag}^2 through the term $(1+\alpha)^2$. Specifically, let d_{tumor} denote the distance of the tumor inside the body, then $d_{\text{tumor}}=d-R_{mag}=\alpha R_{mag}$. Thus to effect particle capture at d_{tumor}, we first compute $\alpha=d_{\text{tumor}}/R_{mag}$, and then use Eq. (73) to compute the minimum particle radius needed for capture. This would seem to imply that noninvasive magnetic drug targeting could be implemented at arbitrary depths in the body by simply choosing a larger magnet. However, recall that the initial position of the particle z_0 needs to be far upstream, outside the influence of the magnet, which occurs when $z_0<-4R_{mag}$. Thus, as R_{mag} increases, the particles need to be injected at a distance that might not be practical. Moreover, R_{mag} is limited to several centimeters for practical rare-earth magnets, and this sets a practical upper limit for d_{tumor}.

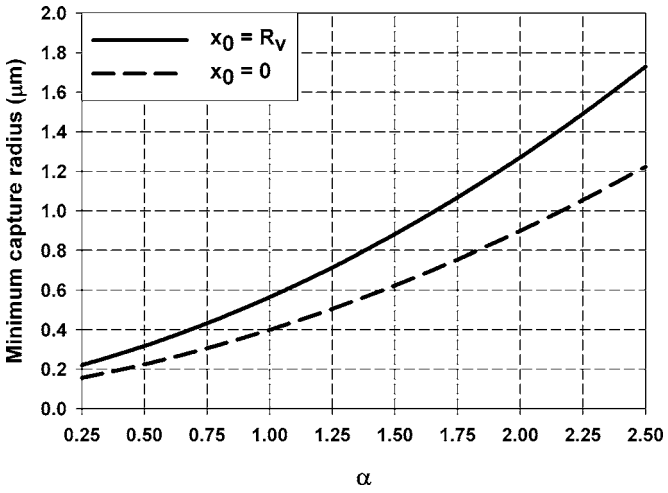

FIG. 9. Minimum particle capture radius for $x_0=Rv$ and $x_0=0$.

IV. CONCLUSION

We have developed an analytical model for predicting the transport and capture of magnetic nanoparticles in the human microcvasulature. The theory applies to noninvasive therapy in which the magnetophoretic control is provided by a cylindrical magnet positioned outside the body. It takes into account the dominant magnetic and fluidic forces that govern particle motion, and is well suited for parametric analysis of practical drug delivery systems for anticancer treatment. We have used the model to study drug delivery, and our results indicate that malignant tissue can be targeted several centimeters within the body using submicron Fe_3O_4 particles. The model developed herein is well suited for the design and optimization of novel magnetophoretic drug targeting apparatus.

[1] F. Marcucci and F. Lefoulon, Drug Discovery Today **9**(5), 219 (2004).
[2] Q. A. Pankhurst, J. Connolly, S. K. Jones, and J. Dobson, J. Phys. D **36**, R167 (2003).
[3] *Scientific and Clinical Applications of Magnetic Carriers*, edited by U. Hafeli, W. Schutt, and J. Teller (Plenum Press, New York, London, 1997).
[4] C. C. Berryl and A. S. G. Curtis, J. Phys. D **36**, R198 (2003).
[5] C. Alexiou, W. Arnold, R. J. Klein, F. G. Parak, P. Hulin, C. Bergemann, C. W. Erhardt, S. Wagenpfeil, and A. S. Lubbe, Cancer Res. **60**, 6641 (2000).
[6] S. Goodwin, C. Peterson, C. Hob, and C. Bittner, J. Magn. Magn. Mater. **194**, 132 (1999).
[7] S. C. Goodwin, C. A. Bittner, C. L. Peterson, and G. Wong, Toxicol. Sci. **60**, 177 (2001).
[8] S. K. Pulfer and J. M. Gallo, J. Drug Target. **6**, 215 (1999).
[9] S. K. Pulfer, S. L. Ciccotto, and J. M. Gallo, J. Neuro-Oncol. **41**, 99 (1999).
[10] A. S. Lubbe, C. Alexiou, and C. Bergemann, J. Surg. Res. **95**(2), 200 (2001).
[11] E. Viroonchatapan *et al.*, Life Sci. **58**, 2251 (1996).
[12] A. S. Lubbe, C. Bergemann, H. Riess, F. Schriever, P. Reichardt, K. Possinger, M. Matthias, B. Doerken, F. Herrmann, and R. Guertler, Cancer Res. **56**, 4686 (1996).
[13] M. O. Aviles, A. D. Ebner, H. T. Chen, A. J. Rosengart, M. D. Kaminski, and J. A. Ritter, J. Magn. Magn. Mater. **293**, 605 (2005).
[14] O. Rotariu, and N. J. C. Strachan, J. Magn. Magn. Mater. **293**, 639 (2005).
[15] H. T. Chen, A. D. Ebner, M. D. Kaminski, A. J. Rosengart, and J. A. Ritter, J. Magn. Magn. Mater. **293**, 616 (2005).
[16] J. A. Ritter, A. D. Ebner, K. D. Daniel, and K. L Stewart, J. Magn. Magn. Mater. **280**, 184 (2004).
[17] T. P. Jones, *Electromechanics of Particles* (Cambridge University Press, Cambridge, UK, 1995).
[18] G. K. Batchelor, *An Introduction in Fluid Dynamics* (Cambridge University Press, London, 1970), p. 233.
[19] R. Gerber, M. Takayasu, and F. J. Friedlander, IEEE Trans. Magn. **19**, 2115 (1983).
[20] M. Takayasu, R. Gerber, and F. J. Friedlander, IEEE Trans. Magn. **19**, 2112 (1983).
[21] D. Fletcher, IEEE Trans. Magn. **27**, 3655 (1991).
[22] E. P. Furlani, *Permanent Magnet and Electromechanical Devices: Materials, Analysis and Applications* (Academic Press, New York, 2001).
[23] A. S. Popel and P. C. Johnson, Annu. Rev. Fluid Mech. **37**, 43 (2005).
[24] A. R. Pries, T. W. Secomb, and P. Gaehtgens, Cardiovasc. Res. **32**, 654 (1996).
[25] A. P. Russell, C. H. Evans, and V. C. Westcott, Biochemistry **164**, 181 (1987).
[26] L. R. Moore, L. Milliron, P. S. Williams, J. J. Chalmers, S. Margel, and M. Zborowski, Anal. Chem. **76**, 3899 (2004).
[27] H. Zhang, M. Zborowski, P. S. Williams, and J. Chalmers, Analyst (Cambridge, U.K.) **130**, 514 (2005).
[28] C. Hunt, B. Moskowitz, and S. Banerjee, in *Rock Physics and Phase Relations, A Handbook of Physical Constants* (American Geophysical Union, Washington, DC, 1995), pp. 189–204.